Emergence of Atypical Properties in Assembled Graphene Nanoribbons

Eduardo Costa Girão,[1,2] Liangbo Liang,[2] Eduardo Cruz-Silva,[2,3] Antônio Gomes Souza Filho,[1] and Vincent Meunier[2]

[1]*Departamento de Física, Universidade Federal do Ceará, Fortaleza, CE, Brazil*

[2]*Department of Physics, Applied Physics, and Astronomy, Rensselaer Polytechnic Institute, Troy, New York 12180, USA*

[3]*Department of Polymer Science and Engineering, University of Massachusetts, Amherst, Massachusetts 01003, USA*

(Received 20 May 2011; published 19 September 2011)

Graphitic nanowiggles (GNWs) are periodic repetitions of nonaligned finite-sized graphitic nanoribbon domains seamlessly stitched together without structural defects. These complex nanostructures have been recently fabricated [Cai *et al.*, Nature (London) **466**, 470 (2010)] and are here predicted to possess unusual properties, such as tunable band gaps and versatile magnetic behaviors. We used first-principles theory to highlight the microscopic origins of the emerging electronic and magnetic properties of the main subclasses of GNWs. Our study establishes a road map for guiding the design and synthesis of specific GNWs for nanoelectronic, optoelectronic, and spintronic applications.

DOI: 10.1103/PhysRevLett.107.135501 PACS numbers: 81.05.ue, 31.15.E−, 75.75.−c

The miniaturization limit of the physical size of Si-based electronics is projected to be reached in a near future. Solid-state alternatives are being investigated in the pursuit of further scaling down of effective operational device structures, while considering increasingly important problems such as heat dissipation and noise associated with reduced dimensionality. In this quest, semiconducting carbon nanosystems seem to be solid front-runner candidates for scaling down to the molecular and atomic sizes. For instance, graphene is a 2D material with great potential to be embedded into electronic nanodevices due to its record-high electronic mobility and low contact resistance [1]. While pristine graphene is not a semiconductor, it can be chemically or structurally modified to acquire suitable semiconducting properties. In that respect, finite width (or graphitic nanoribbons, GNRs) semiconducting sp^2 graphitic materials are known to possess a variable band gap depending on their size and atomic arrangement along their edges [2].

Theory predicts that the properties needed for technological applications of GNRs demand narrow structures (width < 10 nm) with clean edges. To that end, a set of synthesis techniques, including both top-down and bottom-up approaches, has been developed to enable the precise and controlled fabrication of narrow and defect-free systems [3]. Most notably, a block-to-block approach has been recently devised where small aromatic molecules are chemically assembled into highly crystalline narrow ribbons. In this method, a cyclo-dehydrogenation reaction proceeds on a metallic substrate that facilitates both the coupling and the thermally-activated fusion of individual aromatic molecules [4]. This method not only allows for the synthesis of high-quality GNRs, but has also demonstrated the possibility of creating more complex structures, with a variety of shapes such as multiterminal GNRs and other wigglelike one-dimensional systems. Those graphitic nanowiggles (GNWs) are characterized by a periodic repetition of graphene nanoribbon junctions (Fig. 1). Compared to other theoretically proposed structures [5], GNWs are particularly attractive, owing to the existence of a practical synthesis technique. In addition, as we demonstrate in this Letter, GNW nanostructures possess unique properties that are superior to the simple sum of those of their GNR constituents: these atypical properties include electronic and magnetic behaviors which emerge from the interaction between the GNRs building blocks. The present study does not only highlight the general principles guiding the properties of the major possible subclasses of GNWs, it also establishes a road map for the synthesis of GNWs with desired optoelectronic and magnetic behaviors.

We first develop a general framework to classify nanowiggles according to their geometries. We adopt the

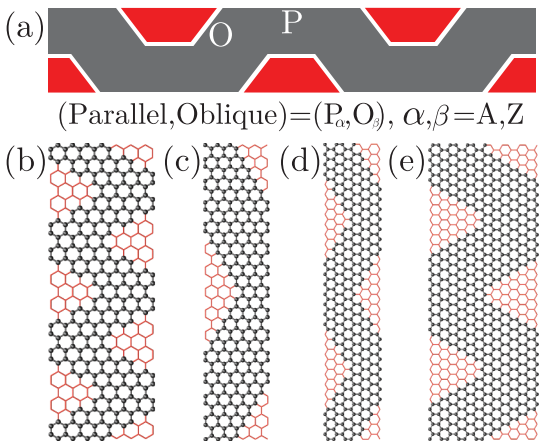

FIG. 1 (color). (a) Geometry and nomenclature of a GNW made up of successive oblique and parallel cuts in armchair (A) or zigzag (Z) patches. (b)–(e) Examples of an (9_A, 6_A) AA (b), (6_A, 7_Z) AZ (c), (4_Z, 9_A) ZA (d) and (7_Z, 7_Z) ZZ (e) GNW. One (c), two (d),(e) and three (b) unit cells of the periodic systems are shown.

conventional notation used for straight nanoribbons. Achiral GNWs can be viewed as an armchair- or zigzag-edged GNR from which trapezoidal wedges [in red on Fig. 1(a)] are symmetrically removed on alternating sides. It is convenient to define the width of the parallel (P_α) and oblique (O_α) sectors by the number of $C-C$ dimer lines ($\alpha = A$) or zigzag strips ($\alpha = Z$) along their width, depending on whether these are armchair or zigzag sectors. The length of an O sector is linearly related to the width of the initial GNR, while the length of the P sector is defined relative to the length of the smallest basis of the neighboring trapezoidal wedge. We adopt a (P_α, O_β) notation to identify each structure uniquely. For example, the nanowiggles reported experimentally in Ref. [4] have a specific geometry made of a periodic combination of A GNR sectors with widths corresponding to (9_A, 6_A), as shown on Fig. 1(b). Here, we will consider an extended set of systems in which the P_α and O_β edges can assume AA [e.g. (9_A, 6_A), Fig. 1(b)], AZ [e.g. (6_A, 7_Z), Fig. 1(c)], ZA [e.g. (4_Z, 9_A), Fig. 1(d)], or ZZ [e.g. (7_Z, 7_Z), Fig. 1(e)] geometries. In this extended set, the length of the O sector is chosen such that at least one full zigzag or armchair strip along the GNW is not cut by the wedges, while the P sector is defined to have the shortest allowed length.

The electronic properties of the systems depicted in Fig. 1 have been calculated within a GGA-based density functional theory (DFT) approach. The DFT calculations were performed with VASP [6]. We computed the electronic properties after full atomic relaxation, using a fine k-point sampling and PAW pseudopotentials, with a cutoff energy of 400 eV for the plane-wave basis set. DFT is too computationally demanding to perform a systematic study of the relationship between the details of the geometry and the electronic properties of GNWs of any size. Fortunately, compared to DFT, the less expensive π-band tight-binding approach yields a good quantitative description of the electronic properties of carbon nanostructures. The present self-consistent tight-binding $+U$ (TBU) calculations are based on the model of Ref. [7] with first-, second-, and third-nearest-neighbor hopping integrals given by $t_1 = 3.2$ eV, $t_2 = 0$ eV and $t_3 = 0.3$ eV, respectively. The different chemical environment at the edges was accounted for by including a $\Delta t_1 = 0.2$ eV correction to the t_1 parameter for the frontier atoms [7]. Further, a precise description of the magnetic interaction in GNRs has been shown to be tractable when the total Hamiltonian includes an explicit Hubbard-like term where spin-spin interactions are treated in a mean-field fashion. This is accomplished by introducing a positive U parameter that quantifies the magnitude of the on-site electron-electron interaction. In practice, this TBU model has been shown to capture the most relevant physical aspects of magnetic states in a number of graphitic systems, including zigzag GNRs [8]. A precise value of the U interaction strength is chosen to match the TBU and DFT band structures for the systems depicted on Fig. 1 considering all their magnetic configurations. The one-parameter fit results in $U = 0.92t_1$. The TBU and DFT results are shown in solid and dashed lines, respectively, in Fig. 2. This figure indicates a remarkable agreement between the DFT and TBU results, and gives us confidence in using the TBU model for the systematic studies performed subsequently. The DFT calculations were performed with edge atoms properly saturated with hydrogen atoms, as implicitly included in the TBU model. We used the model Hamiltonian to study a total of 393 AA, 153 AZ, 75 ZA, and 171 ZZ structures corresponding to a wide range of P and O sector widths [9].

The existence of multiple magnetic states is a major signature of the rich properties of GNWs (Fig. 2). This finding can be rationalized from the properties of individual zigzag and armchair edged GNRs: while armchair systems are nonmagnetic, zigzag systems' ground state is antiferromagnetic [10]. It follows that the AA systems only exist in a nonmagnetic electronic configuration. The large band gap (1.5 eV) observed in the AA GNW of Fig. 1(b) is compatible with the properties of the individual armchair sectors (9_A, 6_A) which present large band gaps since P_A and O_A are multiple of 3 [10]. The energy gaps around the Fermi energy (E_F) are plotted for a variety of AA GNWs as a function of O_A and P_A in Fig. 3(a) (O_A and P_A were

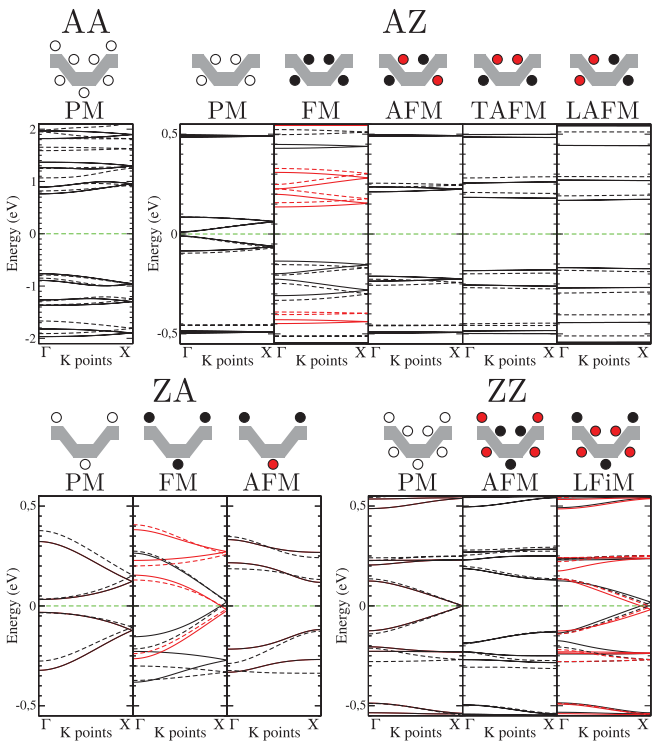

FIG. 2 (color). DFT (dashed lines) and TBU (solid lines) electronic band structures corresponding to the different magnetic states for the representative AA, AZ, ZA and ZZ GNWs shown in Fig. 1. The schematic spin distributions (red: down, black: up) are shown on top of each panel.

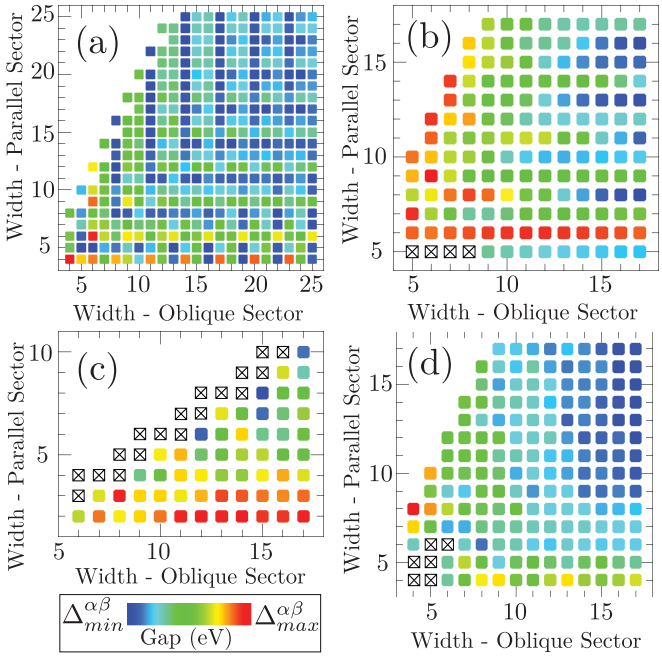

FIG. 3 (color). Energy band gap as a function of P and O for the PM state in AA GNWs (a), and for the AFM state in AZ (b), ZA, (c) and ZZ (d) GNWs. The points absent on the upper-left corner of each graph correspond to geometries not allowed by the particular choice for the lengths of the P and O sectors. For (b)–(d), the systems that do not possess a stable AFM distribution of spins are marked by a cross. In these charts, the band gap minima and maxima are $\Delta^{AA}_{\mathrm{min}} = 1$ meV, $\Delta^{AA}_{\mathrm{max}} = 1.7$ eV, $\Delta^{AZ}_{\mathrm{min}} = 183$ meV, $\Delta^{AZ}_{\mathrm{max}} = 446$ meV, $\Delta^{ZA}_{\mathrm{min}} = 107$ meV, $\Delta^{ZA}_{\mathrm{max}} = 477$ meV, $\Delta^{ZZ}_{\mathrm{min}} = 208$ meV, $\Delta^{ZZ}_{\mathrm{max}} = 491$ meV.

varied from 4 to 25). They can be classified according the multiple-of-three rules, as evidenced by grids evenly spaced in units of 3. The energy gap Δ_N for armchair edged nanoribbons with $N = (3i + j)C - C$ lines follows the relation $\Delta_{3i+1} > \Delta_{3i} > \Delta_{3i+2}$, which also explains why structures with $\mathrm{mod}(P_A, 3) = \mathrm{mod}(O_A, 3) = 2$ possess the smallest gaps [shown in dark blue patterns in Fig. 3(a)].

AZ GNW structures have stable or metastable paramagnetic, ferromagnetic, and antiferromagnetic spin configurations. The specific bands of the $(6_A, 7_Z)$ GNW in Fig. 1(c) are shown in Fig. 2. The paramagnetic (PM) state has four spin-degenerated bands characterized by a very small dispersion (< 0.1 eV) around E_F. Those bands show a two-by-two folded structure relative to the X point in the Brillouin zone. This degeneracy is due to the presence of an improper translation symmetry (translation + C_2 axis in the molecular plane) in the atomistic structure (i.e., the spin distribution displays the full symmetry of the atomic structure, including the order 2 rotation). Deliberate choices of initial guess for the on-site occupations allow the self-consistent process to converge into four different magnetic states. These states are schematically plotted on top of Fig. 2 and their presence can be understood from the properties of individual Z GNRs. The plot highlights the origin of each spin configuration compatible with periodic boundary conditions. They are labeled according to the edge-to-edge spin orientations: ferromagnetic (FM), antiferromagnetic (AFM), trans-anti-ferromagnetic (TAFM), and longitudinal-anti-ferromagnetic (LAFM). In each of those states, the spin polarization is maximal on the zigzag edges, where it has a local ferromagnetic ordering. The polarization decreases quickly from the center of the edges to the corner where the zigzag edge meets the armchair geometry. The FM state presents a splitting between spin-up and -down bands, which opens a $\Delta_{\mathrm{TBU}} = 0.27$ eV ($\Delta_{\mathrm{DFT}} = 0.30$ eV) energy gap. The spin polarized valence state corresponds to the polarization localized at the edges. This polarization is favored while electron-electron interaction pushes the (minority spin) conduction band to higher energy. The other three configurations have no net polarization and their electronic bands are all spin degenerated. The AFM state has a $\Delta_{\mathrm{TBU}} = 0.42$ eV ($\Delta_{\mathrm{DFT}} = 0.46$ eV) band gap, and the bands closest to E_F present very little dispersion, because the spatial spin distribution is restricted to the portion of the nanowiggle with a zigzag edge (e.g., the zigzag portion behaves like a quantum dot, in a way similar to reported antidot graphene [11]). DFT total energy calculations can be used to assess the relative stability of the various phases. Note that in all the systems studied in this work, careful (DFT) geometry relaxation does not yield appreciable differences between the various magnetic states of a given GNW, thereby ruling out the possibility of a spin-Peierls transition. The TBU band-structure energy provides another operational way to compare structure stability. It is easily computed as $E_{\mathrm{TBU}} = \int_{-\infty}^{E_F} En(E)dE$ where $n(E)$ is the density of states. This approximate expression turns out to provide a good predictive framework, compared to the more accurate and computational expensive DFT approach. We found the AFM state to be the most stable: compared to the AFM, DFT (TBU) relative energy is 0.288 eV (0.852 eV) for PM, 0.020 eV (0.027 eV) for TAFM, 0.025 eV (0.027 eV) for LAFM and 0.045 eV (0.046 eV) for FM. Since AFM is the most stable configuration, we performed the systematic band gap study based on that particular spin distribution. The AZ-GNW series considered here spans sector widths P_A and O_Z from 5 to 17 [Fig. 3(b)]. We observe three distinct behaviors corresponding to sector widths P_A such that $\mathrm{mod}(P_A, 3) = 0$, 1, or 2. Moving horizontally across the chart, the electronic band gap oscillates slightly for small O_Z values and gradually converges to a P_A-dependent constant corresponding to the isolated A GNR originated from the wedge-healed GNW. The TAFM and LAFM states present features similar to those mentioned for the AFM configuration. However, the symmetry of the spin distributions in these two last states is reduced since they break the helical symmetry and the degeneracy is lifted at the X point.

Similar to the *AZ* GNW of Fig. 1(c), the PM state of the $(4_Z, 9_A)$ *ZA* GNW system of Fig. 1(d) presents four spin-degenerated bands around E_F. As noted before, these four states can be unfolded in pairs according to the structure's improper translation symmetry. The possible spin configurations include a series of magnetic states with local ferromagnetic alignments along the zigzag edges similar to the *AZ* GNWs. These configurations are either ferromagnetic (FM) or antiferromagnetic (AFM) depending on the relative arrangement of the spin on opposite edges. The FM state has a total magnetic moment of $M_{\mathrm{TBU}} = 1.8\mu_B$ ($M_{\mathrm{DFT}} = 1.9\mu_B$) and is characterized by electronic bands with opposite spins crossing at E_F. In contrast to the PM and FM configurations, the AFM spin distribution breaks the improper translational symmetry of the lattice, and the corresponding bands do not simply fold at the *X* point. However, the symmetry of the spin distribution guarantees a zero total magnetization and, in turn, a spin-degenerate set of bands. The diffraction at the Bragg plane at *X* yields a fairly large $\Delta_{\mathrm{TBU}} = 0.23$ eV ($\Delta_{\mathrm{DFT}} = 0.26$ eV) band gap. In each configuration, the bands around E_F are significantly more dispersed compared to the *AZ* GNW systems, indicating a true 1D behavior and a significant attenuation of the quantum-dot effect observed in the *AZ* GNW considered above. Total energy calculations using DFT (TBU) show that the AFM state is more stable than both the PM and FM configurations, by 0.128 eV (0.438 eV) and 0.057 eV (0.131 eV), respectively. Therefore, our systematic study of *ZA* GNWs focuses on the AFM spin arrangement [Fig. 3(c)] for P_Z and O_A sectors varying from 2 to 10 and 6 to 17, respectively. The general features of the 2D plot show a clear distinction between 3 families as we move along the plot's vertical direction (i.e., as P_Z changes). These three families correspond to different values of O_A such that $\mathrm{mod}(O_A, 3) = 0$, 1, and 2, for reasons similar to those given for the *AZ* systems.

ZZ GNWs constitute the fourth possibility of assembling achiral GNRs into GNWs [Fig. 1(e)]. The PM state is a zero-gap system where the frontier bands meet at the *X* point of the Brillouin zone (Fig. 2). This behavior contrasts with that of straight *Z* GNRs where the frontier bands meet some distance before the *X* point [8,10]. Interestingly, neither DFT nor TBU predict a stable FM state for this particular $(7_Z, 7_Z)$ system. A detailed analysis of the *A* and *B* graphene sublattices explains the absence of a FM state. The coexistence of spin-up along the entire length of the *ZZ* GNW edge would indeed require the local spin on sites belonging to both *A* and *B* sublattices on connected P_Z and O_Z sectors to be aligned. This configuration is not stable for reasonable values of spin-spin interactions. We actually verified that assumption by employing the self-consistent TBU model with an excessively large value of *U* and found the FM state to be artificially stabilized. The *A*-*B* bipartitioning of the lattice does not preclude the presence of other ferromagneticlike spin configurations (see top of Fig. 2). For example, in the AFM state, the edge atoms belonging to a given graphene sublattice present the same type of majority spin. This spin distribution breaks the helical symmetry of the atomic lattice and a $\Delta_{\mathrm{TBU}} = 0.26$ eV ($\Delta_{\mathrm{DFT}} = 0.25$ eV) gap opens at the *X* point. In addition to the AFM spin distribution, the *ZZ* GNWs also allow for a more intriguing longitudinal-ferrimagnetic (LFiM) state as shown on Fig. 3. Because of the quasi-AFM spin distribution (due to the *A*-*B* bipartitionning of the lattice), the total magnetization of LFiM is quite small ($M_{\mathrm{TBU}} = 0.07\mu_B$, $M_{\mathrm{DFT}} = 0.01\mu_B$). However, symmetry arguments do not ensure the total polarization to completely vanish (hence the ferrimagnetic character of the configuration). In addition, except for a small spin-up—spin-down splitting, the LFiM bands are very similar to those of the PM configuration. DFT (TBU) predicts the AFM state to be more stable than the PM or LFiM states, by 0.055 eV (0.446 eV) and 0.056 eV (0.397 eV), respectively. The systematic study of the AFM state for a series of *ZZ* GNWs [Fig. 3(d)] indicates that the band gap changes smoothly as P_Z and O_Z cover the range of values from 4 to 17. The combined variations along the horizontal and vertical directions explain why the gap tends to get smaller along the chart's diagonal to eventually vanish as the 2D graphene character is recovered.

To conclude, our calculations predict the emergence of physical phenomena in experimentally observed GNWs that are absent in their constitutive GNRs. The emergence of these properties is the result of the interplay between the properties of the GNR constituents, the symmetry of the atomic structure, and the bipartition of the graphene lattice. The relationship between the gap and the geometry is dictated by the armchair or zigzag character of the corresponding parallel and oblique sectors, enabling GNWs to offer a broader set of geometrical parameters to tune the electronic structure compared to GNRs. Spin ordering is found to be restricted to zigzag edges, while armchair sectors dictate the formation of magnetic nanodomains whose size can be fine tuned depending on how GNW sectors are assembled. All GNWs with at least one zigzag sector have an antiferromagnetic ground state, in large part due to the bipartition of the graphene lattice. Our calculations also suggest the existence of a number of possible metastable spin distributions, thereby showing GNWs as potential components of spintronic devices. Finally, we anticipate the present study to provide an ideal bridge between the recently synthesized GNWs and their future developments into nanodevices.

E. C. G. acknowledges the Brazilian agency CAPES for the sandwich program fellowship (process 0327-10-7). E. C. S. was supported in part by PHASE, an EFRC funded by the US-DOE under Award Number DE-SC0001087. A. G. S. F. acknowledges support from CNPq and NANOBIOSIMES institute. V. M. was partially supported

by an appointment to the HERE program for faculty at the Oak Ridge National Laboratory (ORNL) administered by ORISE. All the calculations were performed on resources from the Computational Center for Nanotechnology Innovation at RPI.

[1] C.-A. Palma and P. Samori, Nature Chem. **3**, 431 (2011).
[2] I. Deretzis and A. La Magna, Eur. Phys. J. B **81**, 15 (2011).
[3] X. Jia *et al.*, Nanoscale **3**, 86 (2011).
[4] J. Cai *et al.*, Nature (London) **466**, 470 (2010).
[5] Z. F. Wang *et al.*, Appl. Phys. Lett. **91**, 053109 (2007); Y. Hancock *et al.*, J. Low Temp. Phys. **153**, 393 (2008); A. Saffarzadeh and R. Farghadan, Appl. Phys. Lett. **98**, 023106 (2011); H. Sevincli, M. Topsakal, and S. Ciraci, Phys. Rev. B **78**, 245402 (2008); Appl. Phys. Lett. **92**, 173118 (2008).
[6] G. Kresse and J. Furthmüller, Comput. Mater. Sci. **6**, 15 (1996); G. Kresse and J. Furthmüller, Phys. Rev. B **54**, 11 169 (1996).
[7] D. Gunlycke and C. T. White, Phys. Rev. B **77**, 115116 (2008).
[8] O. V. Yazyev, Rep. Prog. Phys. **73**, 056501 (2010).
[9] Other geometrical parameters, such as the length of each sector, could also be varied but we found that the range of properties is well represented by the structures considered here.
[10] Y-. W. Son, M. L. Cohen, and S. G. Louie, Nature (London) **444**, 347 (2006); Phys. Rev. Lett. **97**, 216803 (2006); L. Pisani, J. A. Chan, B. Montanari, and N. M. Harrison, Phys. Rev. B **75**, 064418 (2007).
[11] T. G. Pedersen *et al.*, Phys. Rev. Lett. **100**, 136804 (2008).